

Learning-Based Vulnerability Analysis of Cyber-Physical Systems

Amir Khazraei Spencer Hallyburton Qitong Gao Yu Wang Miroslav Pajic[‡]

Abstract

This work focuses on the use of deep learning for vulnerability analysis of cyber-physical systems (CPS). Specifically, we consider a control architecture widely used in CPS (e.g., in robotics), where the low-level control is based on e.g., the extended Kalman filter (EKF) and an anomaly detector. To facilitate analyzing the impact potential sensing attacks could have, our objective is to develop learning-enabled attack generators capable of designing stealthy attacks that maximally degrade system operation. We show how such problem can be cast within a learning-based grey-box framework where only parts of the runtime information are known to the attacker, and introduce two models based on feed-forward neural networks (FNN) and recurrent neural networks (RNN). Both models are trained offline, using a cost function that combines the attack impact on the estimation error (and thus control) and the residual signal used for anomaly detection, so that the trained models are capable of recursively generating effective yet stealthy sensor attacks in real-time. The effectiveness of the proposed methods is illustrated on several case studies.

1 Introduction

Although many cyber-physical systems (CPS) operate in safety-critical scenarios and the heterogeneous component connectivity provides numerous possible points of attack, most of existing systems are only weakly protected by legacy components, such as anomaly detectors. The challenge of securing CPS is even more formidable as the long system lifetime and resource constraints prevent the full use of new and existing security mechanisms. On the other hand, security-aware resource allocation can significantly reduce the security-related overhead and thus system cost [24, 23, 25]; the idea is to focus on protecting the critical system components and communication links, which if compromised could significantly degrade system performance. Yet, to achieve this, we need methods to analyze system vulnerability, in terms of performance degradation under attack, for different types of attacks.

In this work, we investigate the use of deep learning for the vulnerability analysis of control mechanisms in CPS, focusing on attacks on system sensing. CPS controllers are commonly equipped with a state estimator used for low-level control and anomaly detection. Thus, attacks on sensing may have tremendous impact on the system performance (i.e., quality of control – QoC) by introducing errors in state estimation. In such setting, to maximize the damage by exploiting the compromised components, the goal of the attacker is to modify sensor measurements delivered to the controller such that the system is forced into an unsafe region, while the attack remains undetected (i.e., stealthy).

Consequently, a critical part of the vulnerability analysis are methods/models for design of effective and stealthy attack vectors. Such attack generators should capture how both attack stealthiness and effectiveness are affected by the system dynamics, which in general is nonlinear; this prevents the use of existing model-based methods derived for linear time-invariant systems (e.g., [46, 38, 42, 39]). To address this challenge, we employ deep learning to develop generators of such maximally effective

^{*}Authors are with the Duke University, USA. Emails: {amir.khazraei, spencer.hallyburton, qitong.gao, yu.wang094, miroslav.pajic}@duke.edu.

[†]This work is sponsored in part by the ONR under agreements N00014-17-1-2504 and N00014-20-1-2745, AFOSR under award number FA9550-19-1-0169, as well as the NSF CNS-1652544 award, and a grant from Intel.

yet stealthy attack signals (i.e., time series). Specifically, we provide grey-box yet model-free methods that only use the estimator model (and not the plant model) to train stealthy attack generators. We show that in order to remain stealthy, the attack generator should capture a suitable unstable dynamics, resulting **in large (potentially unbounded) attack vectors over time**; this also prevents the use of standard robustness-based techniques that consider performance degradation in the presence of **bounded** input disturbances. We propose two models for design of the attack vectors; each model requires different levels of runtime information from the state estimator (i.e., the current sensor measurements and the previous state estimation, or only the current sensor measurement). The two models, based on feed-forward neural networks (FNN) and recurrent neural networks (RNN), are trained offline using a cost function that captures the impact the attack would have on the estimation error (and thus QoC) as well as stealthiness requirements. To capture the expectation operation in the cost function, we employ a Monte Carlo (MC) simulation algorithm. Finally, we illustrate the use and evaluate effectiveness of our approach on case studies in the domain of autonomous vehicles.

This work is related in spirit to adversarial machine learning focused on methods to generate adversarial examples that degrade performance of deep neural network (DNN) models. The initial work [41] showed that even small perturbations of DNNs' input could drastically change the output, starting a line of research on vulnerability (in terms of robustness) of DNNs. For instance, [41, 12, 37, 47] study the vulnerability of classifiers by adding a small perturbation z to the input x , and design an adversarial example $x^* = x + z$ that results in miss-classification error $C(x^*) \neq C(x)$, for some classifier C . In [3, 40], the same idea is applied to self-driving vehicles, where the attacker's goal is to fool a DNN perception model into 'detecting' fake objects in front of the vehicle or removing an existing object, in order to maliciously alter its driving decisions. Similarly, [45] extends designing adversarial attacks for regression task where the goal is to add small additive perturbations to alter the predicted geometry of the scene and predicted distances from the camera. Some recent works also consider adversarial machine learning beyond the image domain [26, 48, 9]. For example, [26] studies vulnerability of machine learning models applied in CPS by proposing methods for generating adversarial examples that satisfy some physical constraints.

However, the common assumption among such approaches (e.g., [12, 19, 33, 5, 4, 45, 40, 26, 48, 9]) is that the predicted target only depends on its input and not internal dynamics – i.e., previous states; thus, considering bounded perturbation and a single time-instance (i.e., without longitudinal effects) was sufficient in those cases. On the other hand, to address requirements of attacking a system with internal dynamics, in this work, we show that we *have to consider attack models whose output should also depend on the previous outputs (i.e., previous state)*. In addition, unlike in the aforementioned works, due to the CPS control perspective, both input and outputs belong to a continuous space.

From the control perspective, it has been recently shown that deep reinforcement learning models are susceptible to adversarial examples [44, 27, 13]. Since the mapping between the observation to actions is achieved by a DNN, the idea has been to add small (i.e., bounded) perturbations on observations to alter the actions in a way that minimizes the expected cumulative reward function, even driving the system to unsafe states [44]. On the other hand, in this work, we show that due to the stealthiness constraint, the time series for an effective additive attacks (on sensor measurements) cannot be bounded; rather, the injected attack signal over time should comply with a certain underlying unstable dynamics that depends on the dynamics of the controlled physical process.

Finally, significant efforts focused on model-based (i.e., using more traditional control techniques) design of effective stealthy attacks on CPS controllers [46, 38, 42, 39, 17, 28], including replay [31], covert [38], zero dynamic [42] and false data injection attacks [46]. However, these methods can be used only for linear time-invariant systems, and thus have limited applicability in practice. To the best of our knowledge, this is the first study focused on design of stealthy attack signals – potentially unbounded (in size) vector time-series – that degrade QoC performance of control systems with general nonlinear dynamics, and for which only limited knowledge of the physical model is available.

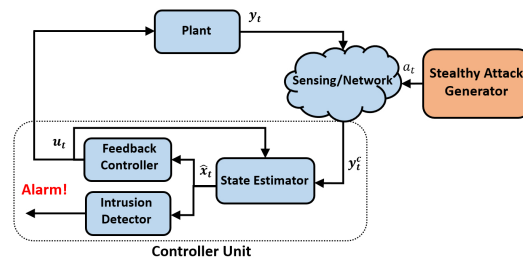


Figure 1: CPS Control architecture under attacks on system sensing – the considered general attack model captures the impact of both network-based attacks (e.g., man-in-the-middle attacks) and direct sensor attacks (e.g., sensor spoofing)

2 Preliminaries

In this section, we formalize the problem considered in this work, starting from the security-aware system (i.e., including the attack) model illustrated in Fig. 1, with each component described in detail. The notation used in this work is captured in Appendix, Section 6.1.

2.1 System Model

We consider general nonlinear dynamics of a physical system (i.e., plant) compromised by an attacker:

$$x_t = f(x_{t-1}, u_{t-1}) + w_{t-1}, \quad y_t^c = y_t + a_t = h(x_t) + v_t + a_t. \quad (1)$$

Here, $x_t \in \mathbb{R}^n$ and $u_t \in \mathbb{R}^m$ denote the plant's state and input vectors at time t , whereas the output vector received by the controller $y_t^c \in \mathbb{R}^p$ contains the measurements from p sensors from the set $\mathcal{S} = \{s_1, \dots, s_p\}$, including compromised measurements provided by sensors from the set $\mathcal{K}_a \subseteq \mathcal{S}$; $a_t \in \mathbb{R}^p$ denotes the attack signal injected at time t , and thus the vector is sparse with support in \mathcal{K}_a – i.e., $\text{supp}(a_t) = \mathcal{K}_a$ and $a_{t,i} = 0$ for $i \in \mathcal{K}_a^c$.³ The observation function $h : \mathbb{R}^n \rightarrow \mathbb{R}^p$ is assumed to be L -Lipschitz. Finally, w_t and v_t are the state and measurement noise. In a special case, if the plant (1) is linear time-invariant (LTI), we use $f(x_t, u_t) = Ax_t + Bu_t$ and $h(x_t) = Cx_t$, where A , B and C are matrices of suitable dimensions.

Control Architecture. We consider a common control architecture, with three main components (as illustrated in Fig. 1): a state estimator, a feedback controller, and an anomaly detector.

The **State Estimator** (observer) employs the system model to predict its (state) evolution, and thus provide an estimate \hat{x}_t of its state at time t ; in general, this can be captured as

$$\hat{x}_t = O_t(\hat{x}_{t-1}, u_{t-1}, y_t), \quad \hat{y}_t = h(\hat{x}_t). \quad (2)$$

The mapping O_t is commonly designed so that (2) minimizes a norm of the estimation error defined as

$$\Delta x_t = x_t - \hat{x}_t. \quad (3)$$

Depending on the system model and statistical characteristics of the noise, different estimation methods are employed. Kalman filters are widely used for LTI systems, whereas Extended Kalman filters (EKFs) are mainly utilized in legacy (and new) nonlinear systems with Gaussian noise, e.g., the autonomous driving and unmanned areal vehicles (UAV) studies considered in this work. Thus, we particularly focus on EKFs. The EKF functionality for a system from (1) is described by

$$\hat{x}_{t|t-1} = f(\hat{x}_{t-1}, u_{t-1}), \quad \hat{x}_t = \hat{x}_{t|t-1} + L_t(y_t - h(\hat{x}_{t|t-1})), \quad \hat{y}_t = h(\hat{x}_t);$$

here, $\hat{x}_{t|t-1}$, \hat{x}_t and \hat{y}_t denote the predicted state estimate, (updated) state estimate, and predicted output, respectively. The EKF gain L_t is also updated as

$$L_t = A_t P_t C_t^T (C_t P_t C_t^T + R)^{-1}, \quad P_{t+1} = A_t P_t A_t^T + Q - L_t (C_t P_t C_t^T + R) L_t^T, \quad (4)$$

where $A_t = \frac{\partial f(x_t, u_t)}{\partial x_t} \big|_{\hat{x}_{t-1}, u_t}$ and $C_t = \frac{\partial h(x_t)}{\partial x_t} \big|_{\hat{x}_{t|t-1}}$ are the Taylor expansion of f and h around (\hat{x}_{t-1}, u_t) and $\hat{x}_{t|t-1}$, respectively. Furthermore, Q and R are the covariance matrix of the Gaussian noises w_t and v_t , respectively. Finally, the residue signal (or innovation noise) is defined as

$$z_t = y_t - h(\hat{x}_{t|t-1}). \quad (5)$$

For systems with Gaussian noise, its covariance matrix is $S_t = \mathbb{E}\{z_t z_t^T\} = C_t P_t C_t^T + R$ [15].

The **Feedback Controller** employs the control law $u_t = \pi(\hat{x}_t)$, and without loss of generality, we assume the control goal is to regulate the states to $0 \in \mathbb{R}^n$. Hence, the estimator (2) can be modeled as

$$\hat{x}_t = O_t(\hat{x}_{t-1}, \pi(\hat{x}_{t-1}), y_t) \triangleq \mathcal{O}_t(\hat{x}_{t-1}, y_t). \quad (6)$$

The **Anomaly Detector** (AD) is used to detect the presence of system anomalies, including intrusions (i.e., attacks). The standard approach is to use the system model to predict the future system behavior and compare it with the actual observation (e.g., see [11] and the references within); capturing the discrepancy between the system and its predicted behavior with a detection function g_t .

³We refer to sensors from \mathcal{K}_a as compromised, even if a sensor itself is not directly compromised, but its measurements may be altered due to e.g., network-based attacks.

In feedback-control based CPS, the residue (5) is widely used for anomaly detection – χ^2 detector in [46, 32], cumulative sum in [43], sequential probability ratio test (SPRT) detector in [22], and a general window-type detector in [14]. For instance, with χ^2 -based detectors the detection function g_t is a weighted norm of z_t (with the χ^2 distribution) – i.e.,

$$g_t = z_t^T S_t^{-1} z_t; \quad (7)$$

the other detectors (e.g., from [21, 22, 32, 20, 43, 46, 29, 30, 14]) use some forms of a windowed extension of (7). Thus, to simplify our presentation, we focus on the detection function g_t from (7), and our results can be directly extended to other cases.

Finally, the system triggers alarm if the detection function satisfies that $g_t > \eta$, for some predefined threshold value η . Usually the value η is assigned such that under normal conditions (i.e., when the system is not compromised) it holds that $\mathbb{P}(g_t > \eta) \leq \epsilon$ – i.e., the system has a low false alarm rate.

2.2 Attack Model

Attacker capabilities during offline training. Let T be the duration of the training phase; we define $\hat{\mathbf{X}}_{t|t-1} = \{\hat{x}_{0|0}, \hat{x}_{1|0}, \dots, \hat{x}_{t|t-1}\}$, $\mathbf{Y}_t = \{y_0, \dots, y_t\}$ and $\mathbf{L}_t = \{L_0, \dots, L_t\}$ as the sequences of the predicted states, plant outputs and EKF gains for $t \geq 0$, with 0 denoting the time starting the training phase. We assume that the attacker has access to the EKF values over time (either directly, or knowing the EKF design and running a copy of the EKF in parallel) – i.e., has access to $\hat{\mathbf{X}}_{T|T-1}$, \mathbf{L}_T , \mathbf{Y}_T and the function h ; specifically, the attacker does not need to know the actual function h , but rather its potential approximation used in (2) to implement the state estimator. Meanwhile, for $0 \leq t < T$, the attacker can compromise the sensor measurements according to (1).

Attacker capabilities at runtime – i.e., during attack. Let t_0 denote the start time of the attack, modeled as in (1), and T' its duration. Again, we assume that the attacker has access to the sensor measurements y_t . In addition, we will consider two scenarios: when the attacker does (i.e., grey-) or does not (i.e., black-box) have access to the state estimation \hat{x}_{t-1} in the previous time step; the latter threat model is especially impactful, as it assumes that the attacker does not have access to the internal controller variables at runtime, but only measurements from the (compromised) system sensors.

Attacker's goal is to *maximize degradation of control performance* – i.e., *QoC*. Specifically, as only sensor data may be compromised, the attack objective is to *maximize the state estimation error* Δx_t . In addition, the attacker wants to *remain stealthy* – i.e., *undetected by the anomaly detector*. These notions are formalized as follows.

Definition 1. *The sequence of attack vectors $a_{t_0}, a_{t_0+1}, \dots$ is referred to as (ϵ, α) -successful if there exists $t' \geq t_0$ such that $\|\Delta x_{t'}\| \geq \alpha$ and $\mathbb{P}(g_t > \eta) \leq \epsilon$ for all $t \geq t_0$.⁴*

Therefore, the attacker's goal is to insert a sequence of false data measurements $a_{t_0}, \dots, a_{t_0+T'}$ resulting in an (ϵ, α) -successful attack. Note that while Def. 1 focuses on attacks that result in a desired norm of the estimation error (i.e., greater than α), for some systems, attacks may cause arbitrarily large estimation errors [14]. For LTI systems with (standard) Kalman filters, the notion of (ϵ, α) -successful attacks was first introduced in [46]. Also, for LTI systems necessary and sufficient conditions such that (ϵ, α) -successful attacks exist for any $\alpha > 0$ are introduced in [46, 21, 14], along with a method to derive such attacks. However, to the best of our knowledge, there is no method for vulnerability analysis of nonlinear systems (1) under sensor-based attacks – i.e., the impact that such attacks would have on the estimation error, and thus QoC.

2.3 Vulnerability Analysis using Learning-Based Attack Design

Therefore, to evaluate the impact that attacks on a subset of sensors \mathcal{K}_a might have on the system, we focus on learning-based attack design for nonlinear dynamical systems described in Sec. 2.1. Specifically, our goal is to develop learning based methods that for any nonlinear system (1), estimator (6), and desired $\alpha > 0$ and $\epsilon < 1$, derive an (ϵ, α) -successful attack sequence if such attack exists.

We start by building intuition about such attacks for LTI systems with Kalman filters, before using it to derive such attacks for nonlinear systems with EKF estimators. Then, we introduce a learning-based methodology to design such attacks for a general type of estimators from (6). To simplify our presentation, in the rest of this work we present the analysis when $\mathcal{K}_a = \mathcal{S}$; still, our methodology can be easily extended to $\mathcal{K}_a \subset \mathcal{S}$, as shown in the case studies.

⁴Note that any p -norm can be used. In this work, when p is not specified, the use of the 2-norm is implied.

3 Adversarial Learning for Nonlinear Dynamical Systems

We start with design of (ϵ, α) -successful attacks against LTI systems with standard Kalman filters.

Lemma 1 ([46, 21, 14]). *For an LTI system with a Kalman filter-based estimator, there exist (ϵ, α) -successful attacks for any desired $\alpha > 0$ if and only if the matrix A is unstable and at least one eigenvector v corresponding to an unstable eigenvalue satisfies that $\text{supp}(Cv) \subseteq \mathcal{K}_a$.*

A being unstable is a necessary condition for existence of (ϵ, α) -successful attack for arbitrarily large α , in LTI systems with Kalman filters. However, if all sensors are under attack (i.e., $\mathcal{K}_a = \mathcal{S}$), this is also a sufficient condition. A similar necessary and sufficient condition **only** for LTI systems with bounded noise that employ novel attack-resilient estimators (e.g., from [8, 36, 35]) is derived in [16].

Now, we show how to use only the current state estimation \hat{x}_t and the plant output y_t to compute such attack sequence on LTI systems for arbitrarily large α .

Theorem 1. *Consider an LTI system with unstable matrix A , and let ϕ_t denote a Gaussian noise vector satisfying $\mathbb{E}\{\phi_t\} = 0$ and $\mathbb{E}\{\phi_t\phi_t^T\} \preceq S$. The attack sequence generated by $a_t = -y_t + CBu_{t-1} + CA\hat{x}_{t-1} + \phi_t$, for $t \geq 0$, is an (ϵ, α) -successful attack for any arbitrary $\alpha > 0$.*

Unlike in design of adversarial examples for images (e.g., [41, 12, 37, 47]), Theorem 1 shows that for LTI dynamical systems, an effective and stealthy attack sequence has to evolve over time (i.e., following suitable dynamics). This inspires us to use a similar structure for generating effective stealthy attacks against system with nonlinear dynamics. Specifically, we consider attacks with dynamics $a_t = F(\hat{x}_{t-1}, y_t)$ (note that y_t and \hat{x}_{t-1} are both functions of a_{t-1}), with the idea to use a DNN to learn F . However, the attacker might not always have access to \hat{x}_{t-1} during the attack; for example, if (s)he used an instance of the system to train the generator, and then uses the derived attack signals to insert attacks over the network without access to the internal execution context of the new system (instance) under attack. Thus, we will consider both the cases where \hat{x}_{t-1} is available and when it is not. For the latter, the idea is to replace \hat{x}_t with another signal r_t that is directly constructed by the attacker. We now summarize our models to design (ϵ, α) -successful attack generators.

FNN-based attack design. When \hat{x}_{t-1} is available to the attacker, we design an FNN that uses the current output measurements and the last state estimation to generate the next attack vector – i.e.,

$$a_t = H_\theta(y_t, \hat{x}_{t-1}), \quad (8)$$

where H_θ is a deep FNN with parameters θ with input dimension of $n + p$ and output dimension p .

RNN-based attack design. When \hat{x}_{t-1} is not available to the attacker, we consider an RNN architecture, that uses only the current sensor measurements for attack design as follows

$$r_t = G_\theta(y_t, r_{t-1}), a_t = Wr_t; \quad (9)$$

here, G_θ is the state update function parameterized by θ , while $W \in \mathbb{R}^{l \times p}$ is a linear mapping from the state r_t to the attack vector a_t . Intuitively, $r_t \in \mathbb{R}^l$ and G_θ should allow for capturing of the evolution of \hat{x}_t , to create a dynamical pattern for the sequence of attack vectors in the RNN design (9).

Model training. To capture the attack impact on the estimation error, the first challenge is that the actual true system state x_t is not available to the attacker; instead, only sensor measurements y_t are known. We show that under some mild assumptions, the sensor measurements can be directly used.

Theorem 2. *If the function $h : \mathbb{R}^n \rightarrow \mathbb{R}^p$ is Lipschitz with constant L , then $\|y_t - h(\hat{x}_t)\| \geq \alpha$ implies $\|x_t - \hat{x}_t\| \geq \frac{\alpha - \sqrt{\sigma k}}{L}$ with probability $1 - \frac{p}{k^2}$, for $k < \frac{\alpha}{\sigma}$ and $R \preceq \sigma I$; here, I is the identity matrix and σ is a positive scalar.*

We use $a_t = F_\theta(y_t, s_{t-1})$ to capture the attack vectors generated by either (8) or (9); here, s_t indicates either r_t or \hat{x}_t . Our goal is to train the parameters in (8) and (9) so that the networks act as generators of (ϵ, α) -successful attacks. To achieve this, we use the following approach.

Starting training at time $t = 0$ we seek for a_0 that maximizes $\mathbb{E}\|x_0 - \hat{x}_0\|^2$ with $\hat{x}_0 = \mathcal{O}(\hat{x}_{-1}, y_0^c)$ and $y_0^c = y_0 + a_0$; here, the expected value operation $\mathbb{E}\{\cdot\}$ is over random variables w and v . As the true state x_0 is not available, from Theorem 2, we can maximize $\mathbb{E}\|y_0 - h(\hat{x}_0)\|^2$ instead. Also, the generated attack should satisfy the stealthiness condition $\mathbb{P}(g_0 > \eta) \leq \epsilon$, with g_0 defined in (7) for

$z_0 = y_0^c - \hat{y}_0$; for χ^2 -based ADs, it holds that $\hat{y}_0 = h(\hat{x}_{0|1})$. Therefore, at time $t = 0$, we solve:

$$\begin{aligned} & \max_{\Theta} \mathbb{E} \|y_0 - h(\hat{x}_0)\|^2 \\ & s.t. \mathbb{P}(g_0 > \eta) \leq \epsilon \\ & a_0 = F_{\Theta}(y_0, s_{-1}). \end{aligned}$$

As this constrained optimization problem is challenging to solve, we penalize the norm of the residue signal and incorporate a new term in our objective function, resulting in the optimization problem:

$$\begin{aligned} & \min_{\Theta} \mathbb{E} \{g_0 - \delta \|y_0 - h(\hat{x}_0)\|^2\} \\ & a_0 = F_{\Theta}(y_0, s_{-1}); \end{aligned} \tag{10}$$

here, $\delta > 0$ is a standard regularization term balancing the stealthiness condition and performance degradation caused by the estimation error.

Let us denote the parameters obtained from (10) as $\Theta^{(0)}$. Now, the attack vector $a_0 = F_{\Theta^{(0)}}(y_0, s_0)$ applied to the sensor measurements at time $t = 0$, would results in state estimate $\hat{x}_0 = \mathcal{O}(\hat{x}_{-1}, y_0^c)$. In the next time step ($t = 1$), we search for parameters such that $\mathbb{E}\{g_1 - \delta \|y_1 - h(\hat{x}_1)\|^2\}$ is minimized. However, in this case the parameters will only be trained to minimize the cost function at time $t = 1$ and thus will disregard minimization of the cost function in the previous time step. Hence, the cost function from the previous time step should be also included – i.e., the objective function to be minimized at time $t = 1$ should be $\mathbb{E}\{g_0 + g_{t_0+1} - \delta (\|y_0 - h(\hat{x}_0)\|^2 + \|y_1 - h(\hat{x}_1)\|^2)\}$.

This approach should continue for the following time steps. Generally, if we consider that the training starts at $t = 0$, for any $t \geq 0$ there should be an instantaneous cost function defined by $J_t = g_t - \delta \|y_t - h(\hat{x}_t)\|$. Therefore, the optimization problem that is solved at time step t is

$$\begin{aligned} & \min_{\Theta} \mathbb{E} \{J_t + \lambda_t \sum_{j=0}^{t-1} J_j\} \\ & a_t = F_{\Theta}(y_t, s_{t-1}). \end{aligned} \tag{11}$$

Again, $\lambda_t \geq 0$ are regularization terms to control the incorporation of previous cost functions. If $\lambda_t = 1$, we effectively penalize all previous and current instantaneous costs equally. For smaller values of λ_t , the cost function at time t will be approximately J_t – i.e., we can do more exploration by only minimizing the cost at time t . However, increasing λ_t helps exploit more by giving more importance to the previous cost functions.

Training Algorithm. In our proposed algorithms, we use Monte Carlo (MC) averaging to approximate the expectation in the cost function (11) by the sample mean over N number of simulated trajectories starting at time $t = 0$. Specifically, the i -th, $i = 1, \dots, N$, trajectory at time t is obtained by

$$x_t^i = f(x_{t-1}^i, u_{t-1}^i) + w_{t-1}^i, \quad y_t^i = h(x_t^i) + v_t^i, \quad \hat{x}_{t|t-1}^i = f(\hat{x}_{t-1}^i, u_{t-1}^i).$$

The cost that the trajectory i at time t imposes is $J_t^i = g_t^i - \delta \|y_t^i - h(\hat{x}_t^i)\|$. However, at time step t the DNN is trained such that $J_t' = \frac{1}{N} \sum_{i=1}^N (\lambda_t \sum_{j=0}^{t-1} J_j^i + J_t^i)$ is minimized, where J_t' is the approximated expectation of cost function in (11). Finally, once the model parameters are obtained at time t , the attack vector $a_t^i = F_{\Theta^{(t)}}(y_t^i, s_{t-1}^i)$ is applied to the system output y_t^i , and the process is repeated until the training completes. When the EKF is used, Algorithm 1 captures pseudocode for learning the FNN-based attack generator (and Alg. 2 in Appendix, Sec. 6.4 for the RNN models).

4 Experiments

We illustrate and evaluate our attack-design framework on three realistic case studies, inverted pendulum, autonomous driving vehicles (ADV) and unmanned aerial vehicles (UAV), with varying level of complexity due to system dynamics. Due to space limitation, the UAV study that considers a very complex (with 12 states), highly nonlinear vehicle dynamics is presented in Appendix, Section 6.7.

4.1 Inverted Pendulum

We assume a fixed based inverted pendulum to illustrate the effectiveness of our algorithm compared to the LTI-based methods from [46, 14]. We used the nonlinear dynamical model of a fixed based inverted pendulum [10]. Two sensors are used to measure the states of the system, θ and $\dot{\theta}$, where θ

Algorithm 1 Stealthy Attack Synthesis Using FNN with MC Simulation

```

1: Set the learning rate  $\beta$ , training period  $T$  and sample number  $N$ 
2: for  $t = 0 : T$  do
3:    $x_t^{1:N} = f(x_{t-1}^{1:N}, u_{t-1}^{1:N}) + w_t^{1:N}$ ,  $y_t^{1:N} = h(x_t^{1:N}) + v_t^{1:N}$ 
4:    $\hat{x}_{t|t-1}^{1:N} = f(\hat{x}_{t-1}^{1:N}, u_{t-1}^{1:N})$ 
5:   repeat
6:      $J'_t = \frac{1}{N} \sum_{i=1}^N (\lambda_t \sum_{j=0}^{t-1} J_j^i + J_t^i)$  with  $y_j^{c1:N} = y_j^{1:N} + H_\theta(\hat{x}_{j-1}^{1:N}, y_j^{1:N})$ 
7:      $\theta^{(t)} \leftarrow \theta^{(t)} - \beta \nabla_{\theta} J'_t$ 
8:   until Convergence
9:    $a_t^{1:N} = H_{\theta^{(t)}}(\hat{x}_{t-1}^{1:N}, y_t^{1:N})$ ,  $y_t^{c1:N} = y_t^{1:N} + a_t^{1:N}$ 
10:   $\hat{x}_t^{1:N} = \hat{x}_{t|t-1}^{1:N} + L_t^{1:N}(y_t^{c1:N} - h(\hat{x}_{t|t-1}^{1:N}))$ ,  $u_t^{1:N} = \pi(\hat{x}_t^{1:N})$ 

```

| SR % FNN/RNN | $\alpha = .5$ | $\alpha = 1$ | $\alpha = 2$ | $\alpha = 4$ | $\alpha = 8$ | $ \theta = \frac{\pi}{8}$ | $ \theta = \frac{\pi}{4}$ | $ \theta = \frac{\pi}{3}$ | $ \theta = \frac{\pi}{2}$ | $ \theta = \pi$ |
|-------------------|---------------|--------------|--------------|--------------|--------------|----------------------------|----------------------------|----------------------------|----------------------------|------------------|
| $T = 50$ | 0/0 | 0/0 | 0/0 | 0/0 | 0/0 | 0/0 | 0/0 | 0/0 | 0/0 | 0/0 |
| $T = 80$ | 100/99 | 26/67 | 0/0 | 0/0 | 0/0 | 0/0 | 0/0 | 0/0 | 0/0 | 0/0 |
| $T = 100$ | 100/100 | 100/100 | 100/78 | 0/3 | 0/0 | 100/81 | 0/9 | 0/0 | 0/0 | 0/0 |
| $T = 120$ | 100/100 | 100/100 | 100/100 | 100/100 | 0/0 | 100/100 | 100/100 | 100/99 | 0/52 | 0/0 |
| $T = 150$ | 100/100 | 100/100 | 100/100 | 100/100 | 89/97 | 100/100 | 100/100 | 100/100 | 100/100 | 50/58 |
| $T = 170$ | 100/100 | 100/100 | 100/100 | 100/100 | 100/100 | 100/100 | 100/100 | 100/100 | 100/100 | 100/100 |
| SR % LTI Model | 100 | 100 | 100 | 10 | 0 | 100 | 14 | 0 | 0 | 0 |

Figure 2: Attack success rate (SR) for different training duration T with $N = 200$, $\lambda = .5$ and varying α and θ over 100 inverted pendulum experiments; FNN/RNN denote FNN vs RNN success rates.

is the angle of pendulum rod from the vertical axis measured counterclockwise. The threshold η is set to have $\epsilon = .01$ (i.e., on average every one hundred time steps a false alarm occurs). A feedback controller is used to keep the pendulum inverted around $\theta = 0$ equilibrium point.

First, we train both FNN and RNN models with $N = 200$ MC samples, $\lambda = .5$ and different values of training period T . The Table in Fig. 2 shows the success rate (in percentage) of both attack models for each training period T and different values of α and θ . For example, consider the entry associated with row $T = 150$ and $\alpha = 8$. It shows that 89 percent of times the FNN and 97 percent of times the RNN model is successful to drive the system to $\alpha = 8$; with α defined as the state estimation error. This definition is also applied to the columns shown by $|\theta|$ (for example the entry in row $T = 150$ and column $|\theta| = \frac{\pi}{2}$ means 100 percent of times both FNN and RNN models are successful to drive the pendulum rod angle to more than $\frac{\pi}{2}$ degrees). We also generated stealthy attacks using the model based LTI method in [46, 14, 21] using the linearized model around the zero equilibrium point.

As summarized, when $T = 50$, neither of the models are successful for any values of α and θ . However, by increasing the values of T , the performance of both attack models improves. Specifically, for $T = 170$ both models are able to drive the pendulum rod to fall without being detected. Moreover, for smaller values of T RNN slightly outperforms FNN, since the RNN is better than FNN *capturing the optimal non-linear attack dynamics in the state-space not explore during the training*. Finally, attacks generated using the LTI model are only successful for $\alpha < 4$ and $\theta < \frac{\pi}{3}$. This shows that the linear model is only effective around the equilibrium point, where the linearization error is small.

The Table in Fig. 5 in Appendix (Sec. 6.5) shows the effect of MC sample number on the attack model performance for a fixed $T = 150$ – for smaller values of N , FNN performs better, however, when both models have enough data (e.g., $N \geq 250$) both models work equally well. Similarly, the Table in Fig. 6 in Appendix (Sec. 6.5), shows how different values of λ in training phase affect the attack model performance. We show that for smaller values of λ , RNN works poorly as the data in previous time steps are important to train the model, accurately capturing the desired attack dynamics.

4.2 Autonomous Driving Vehicles

Generic Vehicle Model. We first considered a simple nonlinear dynamical model of ADV from [18], with four states $[x \ y \ \psi \ v]^T$; here, x and y represent the position of the center of mass in x and y axis, respectively, ψ is the inertial heading, and v is the velocity of the vehicle. The states x, y, ψ are measured using noisy sensors, with zero-mean noise with covariance matrix $R = .01I$. The system noise is zero-mean, with covariance $Q = .001I$ and we set the threshold η to have $\epsilon = .01$.

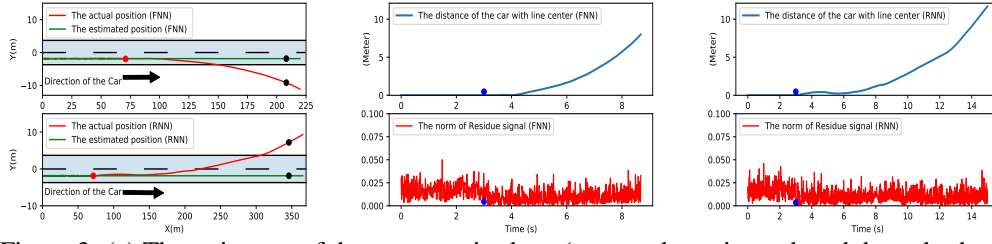


Figure 3: (a) The trajectory of the compromised car (green - the estimated, and the red - the actual vehicle position; the red dot shows the place where the attack starts, the black dots show the actual and estimated position of the car at the same time). (b,c) The above sub-figures show the distance of the car with the center of the lane. The below sub-figures illustrate the norm of residue signal before and after the start time of attack $t = 3s$ (the blue dots) for each FNN and RNN-based generators.

Table 1: Attack success rate (SR) for different values of training duration T with $N = 200$, $\lambda = .5$ and different values of α and y over 100 experiments for AV.

| SR % FNN/RNN | $ y = .2$ | $ y = 1$ | $ y = 2$ | $ y = 4$ | $ y = 6$ | $ y = 8$ | $ y = 10$ | $ y = 14$ |
|-----------------|------------|-----------|-----------|-----------|-----------|-----------|------------|------------|
| $T = 100$ | 100/100 | 0/0 | 0/0 | 0/0 | 0/0 | 0/0 | 0/0 | 0/0 |
| $T = 200$ | 100/100 | 98/100 | 16/0 | 0/0 | 0/0 | 0/0 | 0/0 | 0/0 |
| $T = 300$ | 100/100 | 100/100 | 100/100 | 32/100 | 0/0 | 0/0 | 0/0 | 0/0 |
| $T = 500$ | 100/100 | 100/100 | 100/100 | 100/99 | 100/99 | 50/96 | 23/96 | 0/0 |
| $T = 700$ | 100/100 | 100/100 | 100/100 | 100/100 | 100/100 | 100/100 | 100/100 | 82/99 |

We assume the car has a constant speed of $25m/s$ and a feedback controller is used to keep the car between the lanes. We train offline the FNN and RNN models for generating stealthy attacks. The network H_θ is fully connected with 20 neurons and the ReLU activation function, whereas G_θ is an RNN with one layer and 20 neurons and the ReLU activation function. First, we train both models with $N = 200$ MC samples, $\lambda = .5$ and different values of training period T . Table 1 shows the success rate (in percentage) of both attack models for each training period T and different values of α and $|y|$, the car’s distance from the center of the lane). As summarized, increasing the attack duration helps driving the system towards the unsafe region (i.e., increasing $|y|$). Also, the attacks generated by the RNN model outperform the FNN ones in driving the vehicle to the unsafe region. We also analyzed the impact of N , the MC sampling number during training, on attack performance (Table 2 in Appendix, Section 6.6); we showed that using $N \geq 100$ in training is sufficient.

Fig. 2a shows the trajectory of the car. Before starting the attack at the location $X = 75m$, the car (blue line) is moving between the lanes and the estimated trajectory (green line) has a very small estimation error. However, using either attacks derived by the FNN or RNN-based attack generators, the car is being pushed off the road while the estimated position shows that the car is still in the road. Furthermore, the attacks are stealthy – the anomaly detector cannot detect the presence of either of the attacks. Fig. 2b and Fig. 2c show the estimation error along the X and Y axis for these scenarios.

Real-World Autonomous Driving Simulator – Evaluating on CARLA. To evaluate our methodology on complex, realistic systems, for which we do not know the model of the highly non-linear vehicle dynamics, we used ADV scenarios in the vehicle simulator CARLA [6] built on Unreal Engine 4, and providing realistic physics and sensor models in complex urban environments with static and dynamic actors. We define a planning-navigation-control loop that drives the autonomous vehicle, leveraging the EKF structure for chi-square anomaly detector; CARLA setup details are presented in Appendix, Section 6.6.1 and the videos of our CARLA experiments are available at [1].

We evaluate our FNN and RNN attack-generators for *performance and generalizability*, and compare to the nominal case, i.e., without attacks. We illustrate that both FNN and RNN-based attack generators are able to drive the vehicle into unsafe situations (e.g., crashes into other cars or static objects) over short times while remaining undetected. We highlight here the results when not all of the sensors are compromised (i.e., $\mathcal{K}_a \neq \mathcal{S}$) – i.e., when the FNN and RNN-based attack generator *are only be able to attack GNSS position measurements and to only have knowledge of positions states* (i.e., no knowledge of velocity or heading). Despite these restrictions, both attack generators

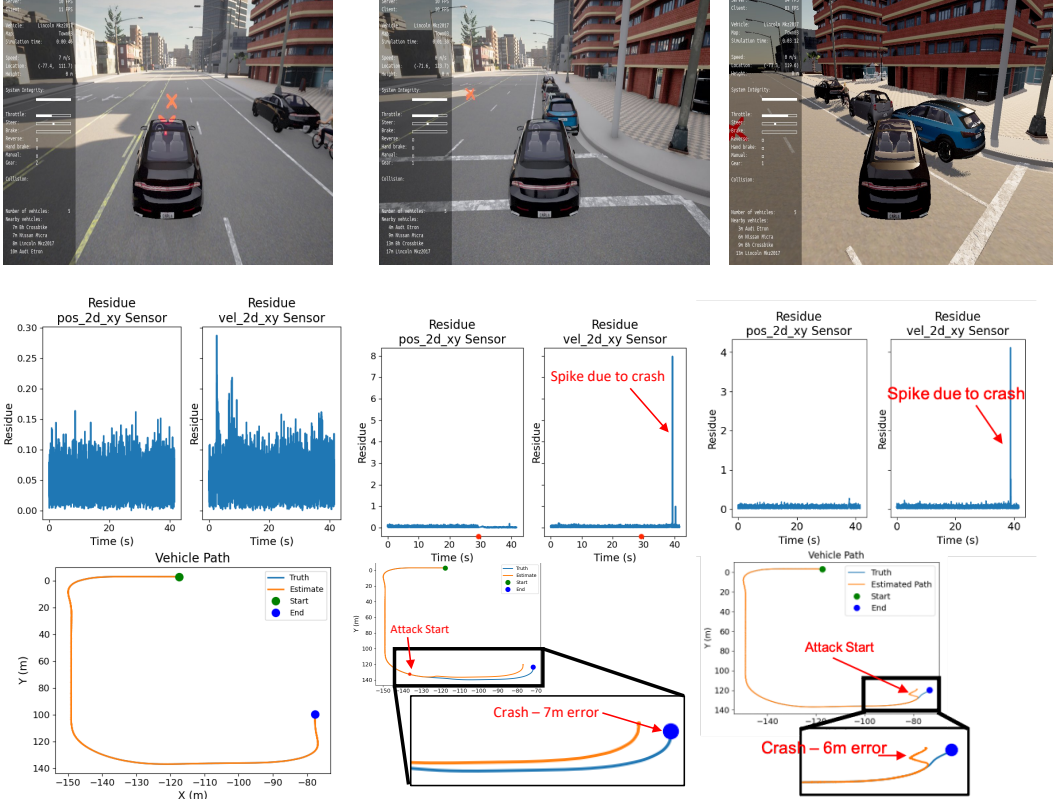


Figure 4: (a) CARLA simulation when the car is free of attack; (b,c) The vehicle collisions with off-road objects due to the injecting sensor attacks using the FNN and RNN-based attack generators, respectively; (d) The vehicle trajectory without attack and the residue signals for both velocity and position sensors; (e,f) The trajectory when the position sensors are compromised using the FNN and RNN-based methods, respectively, and the corresponding residue signals.

produce stealthy attacks that significantly move the vehicle off-course (e.g., resulting in a collision).

Additionally, we demonstrated the attack generalizability twofold. First, we train the FNN and RNN-based models offline on a simple path (i.e., not the testing path). We then test those same models on the full CARLA environment and paths. Second, we demonstrated the proof-of-concept that our attack models are able to generalize to different rates of sensor data by training at 100 Hz measurements and testing at 120 Hz measurements and retaining attack stealthiness and effectiveness. Fig. 4 presents some of the results. Specifically, Fig. 4d shows the path and residue values when the sensors are NOT under attack. Fig. 4e and Fig. 4f show the path and the residue signal values of the compromised car when the FNN and RNN-based generators are used to create inserted attack signals. The endpoint of the path is when the car hits an object and stops moving. Note that the residue signal has a huge spike only when the car hits the object (due to the collision), too late for any recovery action.

5 Conclusion

In this work, we have utilized deep learning to generate stealthy attacks on control components in cyber-physical systems, focusing on a widely used architecture where the low-level control is based on the extended Kalman filter and an anomaly detector. We have considered a grey box setup, with unknown nonlinear plant dynamics and known observation functions and Kalman filter gains. We have shown that feedforward and recurrent neural networks (FNN and RNN, respectively) can be used to generate stealthy adversarial attacks on sensing information delivered to the system, resulting in large errors to the estimates of the state of the system without being detected. Both FNN and RNN are trained offline from a cost function combining the attack effects on the estimation error and the residual signal of the EKF; thus, the trained model is capable of recursively generating such effective sensor attacks in real-time using only current sensor measurements. The effectiveness of the proposed methods has been illustrated and evaluated on several case studies, with varying complexity.

References

- [1] Video, CARLA Case Study. https://drive.google.com/drive/folders/1uLd8D4WmVy_GpBXpuJW_G0u6bNtD4Ltj. Accessed: 2021-04-30.
- [2] S. Bouabdallah and R. Siegwart. Full control of a quadrotor. In *2007 IEEE/RSJ International Conference on Intelligent Robots and Systems*, pages 153–158. Ieee, 2007.
- [3] Y. Cao, C. Xiao, B. Cyr, Y. Zhou, W. Park, S. Rampazzi, Q. A. Chen, K. Fu, and Z. M. Mao. Adversarial sensor attack on lidar-based perception in autonomous driving. In *Proceedings of the 2019 ACM SIGSAC conference on computer and communications security*, pages 2267–2281, 2019.
- [4] N. Carlini and D. Wagner. Towards evaluating the robustness of neural networks. In *2017 IEEE Symposium on Security and Privacy (SP)*, pages 39–57. IEEE, 2017.
- [5] F. Croce and M. Hein. Minimally distorted adversarial examples with a fast adaptive boundary attack. In *International Conference on Machine Learning*, pages 2196–2205. PMLR, 2020.
- [6] A. Dosovitskiy, G. Ros, F. Codevilla, A. Lopez, and V. Koltun. Carla: An open urban driving simulator. In *Conference on robot learning*, pages 1–16. PMLR, 2017.
- [7] M. T. Emirler, İ. M. C. Uygan, B. Aksun Güvenç, and L. Güvenç. Robust pid steering control in parameter space for highly automated driving. *International Journal of Vehicular Technology*, 2014, 2014.
- [8] H. Fawzi, P. Tabuada, and S. Diggavi. Secure estimation and control for cyber-physical systems under adversarial attacks. *IEEE Transactions on Automatic control*, 59(6):1454–1467, 2014.
- [9] C. Feng, T. Li, Z. Zhu, and D. Chana. A Deep Learning-based Framework for Conducting Stealthy Attacks in Industrial Control Systems. *arXiv:1709.06397 [cs]*, 2017.
- [10] A. Formal’skii. An inverted pendulum on a fixed and a moving base. *Journal of applied mathematics and mechanics*, 70(1):56–64, 2006.
- [11] J. Giraldo, D. Urbina, A. Cardenas, J. Valente, M. Faisal, J. Ruths, N. O. Tippenhauer, H. Sandberg, and R. Candell. A survey of physics-based attack detection in cyber-physical systems. *ACM Computing Surveys (CSUR)*, 51(4):1–36, 2018.
- [12] I. J. Goodfellow, J. Shlens, and C. Szegedy. Explaining and harnessing adversarial examples. *arXiv preprint arXiv:1412.6572*, 2014.
- [13] S. Huang, N. Papernot, I. Goodfellow, Y. Duan, and P. Abbeel. Adversarial attacks on neural network policies. *arXiv preprint arXiv:1702.02284*, 2017.
- [14] I. Jovanov and M. Pajic. Relaxing integrity requirements for attack-resilient cyber-physical systems. *IEEE Transactions on Automatic Control*, 64(12):4843–4858, Dec 2019. ISSN 2334-3303. doi: 10.1109/TAC.2019.2898510.
- [15] S. J. Julier and J. K. Uhlmann. Unscented filtering and nonlinear estimation. *Proceedings of the IEEE*, 92(3):401–422, 2004.
- [16] A. Khazraei and M. Pajic. Perfect attackability of linear dynamical systems with bounded noise. In *2020 American Control Conference (ACC)*, pages 749–754, 2020.
- [17] A. Khazraei, H. Kebriaei, and F. R. Salmasi. A new watermarking approach for replay attack detection in lqg systems. In *56th IEEE Annual Conf. on Decision and Control (CDC)*, pages 5143–5148, 2017.
- [18] J. Kong, M. Pfeiffer, G. Schildbach, and F. Borrelli. Kinematic and dynamic vehicle models for autonomous driving control design. In *2015 IEEE Intelligent Vehicles Symposium (IV)*, pages 1094–1099. IEEE, 2015.
- [19] A. Kurakin, I. Goodfellow, and S. Bengio. Adversarial examples in the physical world. *arXiv preprint arXiv:1607.02533*, 2016.
- [20] C. Kwon and I. Hwang. Reachability analysis for safety assurance of cyber-physical systems against cyber attacks. *IEEE Transactions on Automatic Control*, 63(7):2272–2279, 2017.
- [21] C. Kwon, W. Liu, and I. Hwang. Analysis and design of stealthy cyber attacks on unmanned aerial systems. *Journal of Aerospace Information Systems*, 11(8):525–539, 2014.
- [22] C. Kwon, S. Yantek, and I. Hwang. Real-time safety assessment of unmanned aircraft systems against stealthy cyber attacks. *Journal of Aerospace Information Systems*, 13(1):27–45, 2016.

- [23] V. Lesi, I. Jovanov, and M. Pajic. Network scheduling for secure cyber-physical systems. In *2017 IEEE Real-Time Systems Symposium (RTSS)*, pages 45–55, Dec 2017. doi: 10.1109/RTSS.2017.00012.
- [24] V. Lesi, I. Jovanov, and M. Pajic. Security-aware scheduling of embedded control tasks. *ACM Trans. Embed. Comput. Syst.*, 16(5s):188:1–188:21, Sept. 2017. ISSN 1539-9087. doi: 10.1145/3126518. URL <http://doi.acm.org/10.1145/3126518>.
- [25] V. Lesi, I. Jovanov, and M. Pajic. Integrating security in resource-constrained cyber-physical systems. *ACM Trans. Cyber-Phys. Syst.*, 4(3), May 2020. ISSN 2378-962X. doi: 10.1145/3380866. URL <https://doi.org/10.1145/3380866>.
- [26] J. Li, J. Y. Lee, Y. Yang, J. S. Sun, and K. Tomsovic. ConAML: Constrained Adversarial Machine Learning for Cyber-Physical Systems. *arXiv:2003.05631 [cs]*, 2020.
- [27] Y.-C. Lin, Z.-W. Hong, Y.-H. Liao, M.-L. Shih, M.-Y. Liu, and M. Sun. Tactics of adversarial attack on deep reinforcement learning agents. In *Proceedings of the 26th International Joint Conference on Artificial Intelligence*, pages 3756–3762, 2017.
- [28] Y. Liu, P. Ning, and M. K. Reiter. False data injection attacks against state estimation in electric power grids. *ACM Transactions on Information and System Security (TISSEC)*, 14(1):1–33, 2011.
- [29] F. Miao, M. Pajic, and G. Pappas. Stochastic game approach for replay attack detection. In *IEEE 52nd Annual Conference on Decision and Control (CDC)*, pages 1854–1859, Dec 2013. doi: 10.1109/CDC.2013.6760152.
- [30] F. Miao, Q. Zhu, M. Pajic, and G. J. Pappas. Coding schemes for securing cyber-physical systems against stealthy data injection attacks. *IEEE Transactions on Control of Network Systems*, 4(1):106–117, March 2017. ISSN 2372-2533. doi: 10.1109/TCNS.2016.2573039.
- [31] Y. Mo and B. Sinopoli. Secure control against replay attacks. In *47th Annual Allerton Conference on Communication, Control, and Computing*, pages 911–918. IEEE, 2009.
- [32] Y. Mo and B. Sinopoli. On the performance degradation of cyber-physical systems under stealthy integrity attacks. *IEEE Transactions on Automatic Control*, 61(9):2618–2624, 2015.
- [33] S.-M. Moosavi-Dezfooli, A. Fawzi, and P. Frossard. Deepfool: a simple and accurate method to fool deep neural networks. In *Proceedings of the IEEE conference on computer vision and pattern recognition*, pages 2574–2582, 2016.
- [34] J. Navarro. A very simple proof of the multivariate chebyshev’s inequality. *Communications in Statistics-Theory and Methods*, 45(12):3458–3463, 2016.
- [35] M. Pajic, I. Lee, and G. J. Pappas. Attack-resilient state estimation for noisy dynamical systems. *IEEE Transactions on Control of Network Systems*, 4(1):82–92, March 2017. ISSN 2372-2533. doi: 10.1109/TCNS.2016.2607420.
- [36] M. Pajic, J. Weimer, N. Bezzo, O. Sokolsky, G. J. Pappas, and I. Lee. Design and implementation of attack-resilient cyberphysical systems: With a focus on attack-resilient state estimators. *IEEE Control Systems Magazine*, 37(2):66–81, April 2017. ISSN 1941-000X. doi: 10.1109/MCS.2016.2643239.
- [37] N. Papernot, P. McDaniel, I. Goodfellow, S. Jha, Z. B. Celik, and A. Swami. Practical black-box attacks against machine learning. In *Proceedings of the 2017 ACM on Asia conference on computer and communications security*, pages 506–519, 2017.
- [38] R. S. Smith. Covert misappropriation of networked control systems: Presenting a feedback structure. *IEEE Control Systems Magazine*, 35(1):82–92, 2015.
- [39] T. Sui, Y. Mo, D. Marelli, X.-M. Sun, and M. Fu. The vulnerability of cyber-physical system under stealthy attacks. *IEEE Transactions on Automatic Control*, 2020.
- [40] J. Sun, Y. Cao, Q. A. Chen, and Z. M. Mao. Towards robust lidar-based perception in autonomous driving: General black-box adversarial sensor attack and countermeasures. In *29th {USENIX} Security Symposium ({USENIX} Security 20)*, pages 877–894, 2020.
- [41] C. Szegedy, W. Zaremba, I. Sutskever, J. Bruna, D. Erhan, I. Goodfellow, and R. Fergus. Intriguing properties of neural networks. *arXiv preprint arXiv:1312.6199*, 2013.

- [42] A. Teixeira, I. Shames, H. Sandberg, and K. H. Johansson. Revealing stealthy attacks in control systems. In *2012 50th Annual Allerton Conference on Communication, Control, and Computing (Allerton)*, pages 1806–1813. IEEE, 2012.
- [43] R. Tunga, C. Murguia, and J. Ruths. Tuning windowed chi-squared detectors for sensor attacks. In *2018 Annual American Control Conference (ACC)*, pages 1752–1757. IEEE, 2018.
- [44] T.-W. Weng, K. D. Dvijotham*, J. Uesato*, K. Xiao*, S. Gowal*, R. Stanforth*, and P. Kohli. Toward evaluating robustness of deep reinforcement learning with continuous control. In *International Conference on Learning Representations*, 2020. URL <https://openreview.net/forum?id=SylL0krYPS>.
- [45] A. Wong, S. Cicek, and S. Soatto. Targeted adversarial perturbations for monocular depth prediction. *Advances in Neural Information Processing Systems*, 33, 2020.
- [46] Y. Mo and B. Sinopoli. False data injection attacks in control systems. In *First workshop on Secure Control Systems*, pages 1–6, 2010.
- [47] X. Yuan, P. He, Q. Zhu, and X. Li. Adversarial examples: Attacks and defenses for deep learning. *IEEE transactions on neural networks and learning systems*, 30(9):2805–2824, 2019.
- [48] G. Zizzo, C. Hankin, S. Maffei, and K. Jones. Adversarial Machine Learning Beyond the Image Domain. In *Proceedings of the 56th Annual Design Automation Conference 2019*, pages 1–4, 2019.

6 Appendix

6.1 Notation

\mathbb{R} denotes the set of real numbers, whereas \mathbb{P} and \mathbb{E} denote the probability and expectation for a random variable. For a matrix A , A^T denotes its transpose and for a square matrix $\text{trace}(A)$ denotes the trace of the matrix A . In addition, I is the identity matrix in general, while I_p denotes the identity matrix with dimension $p \times p$ (i.e., $I_p \in \mathbb{R}^{p \times p}$). Matrix $A \in \mathbb{R}^{n \times n}$ is positive semidefinite, which is denoted by $A \succeq 0$, if $x^T A x \geq 0$ holds for all $x \in \mathbb{R}^n$. For two positive semidefinite matrices A and B , we denote by $A \preceq B$ if it holds that $(B - A) \succeq 0$. For a vector $x \in \mathbb{R}^n$, we denote by $\|x\|_p$ the p -norm of x ; when p is not specified, the 2-norm is implied. In addition, $\text{supp}(x)$ denotes the indices of the nonzero elements of $x \in \mathbb{R}^n$ – i.e., $\text{supp}(x) = \{i \mid i \in \{1, \dots, n\}, x_i \neq 0\}$. Finally, a function $h : \mathbb{R}^n \rightarrow \mathbb{R}^p$ is L-Lipschitz if for any $x, y \in \mathbb{R}^n$ it holds that $\|h(x) - h(y)\| \leq L\|x - y\|$.

6.2 Proof of Theorem 1

First, we will show that applying such attack sequence results in an unbounded estimation error. For LTI systems, the dynamic of the state estimation error follows

$$\begin{aligned} \Delta x_t &= x_t - \hat{x}_t \\ &= A\Delta x_{t-1} + w_t - L(y_t^c - CA\hat{x}_{t-1} - CBu_{t-1}) \\ &= A\Delta x_{t-1} + w_t - L\phi_t \end{aligned}$$

As the matrix A is unstable, it follows that $\|\Delta x_t\|$ will be unbounded as $t \rightarrow \infty$.

We now show that the attack is stealthy from the perspective of the IDS. In this case, the residue signal z_t satisfies

$$\begin{aligned} z_t &= y_t^c - C(A\hat{x}_{t-1} + Bu_{t-1}) = \\ &= y_t + a_t - C(A\hat{x}_{t-1} + Bu_{t-1}) = \phi_t. \end{aligned} \tag{12}$$

Therefore, it follows that

$$\begin{aligned} \mathbb{E}\{g_t^a\} &= \mathbb{E}\{z_t^T S^{-1} z_t\} = \mathbb{E}\{\phi_t^T S^{-1} \phi_t\} \\ &= \text{trace}(\mathbb{E}\{\phi_t^T S^{-1} \phi_t\}) = \mathbb{E}\{\text{trace}(\phi_t \phi_t^T S^{-1})\} \\ &= \text{trace}(\mathbb{E}\{\phi_t \phi_t^T\} S^{-1}) \leq \text{trace}(SS^{-1}) = p, \end{aligned}$$

where we used the linearity of expectation and trace operation. Note that for LTI systems, the expectation of g_t (also known as the degrees of freedom of the distribution) satisfies that $\mathbb{E}\{g_t\} = p$. Based on the properties of the χ^2 distribution, since $\mathbb{E}\{g_t^a\} \leq \mathbb{E}\{g_t\} = p$, it follows that $\mathbb{P}(g_t^a > \eta) \leq \mathbb{P}(g_t > \eta) = \epsilon$, and thus the attack sequence is stealthy.

Algorithm 2 Stealthy Attack Synthesis Using RNN with MC Simulation

```

1: Set the learning rate  $\beta$ , training period  $T$  and sample number  $N$ 
2: for  $t = 0 : T$  do
3:    $x_t^{1:N} = f(x_{t-1}^{1:N}, u_{t-1}^{1:N}) + w_{t-1}^{1:N}$ 
4:    $y_t^{1:N} = h(x_t^{1:N}) + v_t^{1:N}$ 
5:    $\hat{x}_{t|t-1}^{1:N} = f(\hat{x}_{t-1}^{1:N}, u_{t-1}^{1:N})$ 
6:   repeat
7:      $J'_t = \frac{1}{N} \sum_{i=1}^N (\lambda_t \sum_{j=0}^{t-1} J_j^i + J_t^i)$  with  $y_t^{c1:N} = y_j^{1:N} + W G_\theta(r_{j-1}^{1:N}, y_j^{1:N})$ 
8:      $\theta^{(t)} \leftarrow \theta^{(t)} - \beta \nabla_{\theta} J'_t$ 
9:      $W^{(t)} \leftarrow W^{(t)} - \beta \nabla_W J'_t$ 
10:  until Convergence
11:   $r_t^{1:N} = G_{\theta^{(t)}}(r_{t-1}^{1:N}, y_t^{1:N})$ 
12:   $a_t^{1:N} = W^{(t)} r_t^{1:N}$ 
13:   $y_t^{c1:N} = y_t^{1:N} + a_t^{1:N}$ 
14:   $\hat{x}_t^{1:N} = \hat{x}_{t|t-1}^{1:N} + L_t^{1:N} (y_t^{c1:N} - h(\hat{x}_{t|t-1}^{1:N}))$ 
15:   $u_t^{1:N} = \pi(\hat{x}_t^{1:N})$ 

```

| SR % FNN/RNN | $\alpha = .5$ | $\alpha = 1$ | $\alpha = 2$ | $\alpha = 4$ | $\alpha = 8$ | $ \theta = \frac{\pi}{8}$ | $ \theta = \frac{\pi}{4}$ | $ \theta = \frac{\pi}{3}$ | $ \theta = \frac{\pi}{2}$ | $ \theta = \pi$ |
|-----------------|---------------|--------------|--------------|--------------|--------------|----------------------------|----------------------------|----------------------------|----------------------------|------------------|
| $N = 1$ | 35/4 | 35/2 | 35/1 | 35/1 | 10/0 | 35/1 | 35/1 | 35/1 | 35/0 | 0/0 |
| $N = 10$ | 100/19 | 100/10 | 100/4 | 100/2 | 45/1 | 100/4 | 100/2 | 100/1 | 100/1 | 0/0 |
| $N = 50$ | 100/74 | 100/66 | 100/56 | 100/38 | 100/4 | 100/56 | 100/39 | 100/32 | 100/9 | 0/0 |
| $N = 100$ | 100/96 | 100/96 | 100/96 | 100/95 | 90/64 | 100/96 | 100/96 | 100/95 | 100/90 | 15/1 |
| $N = 250$ | 100/100 | 100/100 | 100/100 | 100/100 | 95/97 | 100/100 | 100/100 | 100/100 | 100/100 | 94/95 |
| $N = 500$ | 100/100 | 100/100 | 100/100 | 100/100 | 100/100 | 100/100 | 100/100 | 100/100 | 100/100 | 100/99 |

Figure 5: Attack success rate (SR) for different values of N with $T = 150$, $\lambda = .5$ and different values of α and θ over 100 experiments for the inverted pendulum. The FNN/RNN numbers denote FNN vs RNN success rate values.

6.3 Proof of Theorem 2

From the multivariate Chebyshev's inequality [34], it holds that $\mathbb{P}(v_t^T R^{-1} v_t \leq k^2) \geq 1 - \frac{p}{k^2}$. On the other hand, using our assumption $R \preceq \sigma I$, it holds that $\sigma^{-1} v_t^T v_t \leq v_t^T R^{-1} v_t$ for any $v_t \in \mathbb{R}^p$. Therefore, $\mathbb{P}(v_t^T v_t \leq \sigma k^2) \geq 1 - \frac{p}{k^2}$ or equivalently $\mathbb{P}(\|v_t\| \leq \sqrt{\sigma} k) \geq 1 - \frac{p}{k^2}$. Now, with the probability of at least $1 - \frac{p}{k^2}$, we have that

$$\begin{aligned}
\alpha &\leq \|y_t - h(\hat{x}_t)\| = \|h(x_t) + v_t - h(\hat{x}_t)\| \leq \\
&\leq L\|x_t - \hat{x}_t\| + \|v_t\| \leq L\|x_t - \hat{x}_t\| + \sqrt{\sigma} k,
\end{aligned}$$

which results in $\|x_t - \hat{x}_t\| \geq \frac{\alpha - \sqrt{\sigma} k}{L}$.

6.4 Algorithm 2

Due to the space limitation, we provide the Alg. 2 in this section. This algorithm captures pseudocode for learning the RNN-based attack generator.

6.5 Inverted Pendulum

The Table in Fig. 5 shows the effect of MC sample number on the attack model performance for a fixed $T = 150$ – for smaller values of N , FNN performs better, however, when both models have enough data (e.g., $N \geq 250$) both models work equally well. Similarly, the Table in Fig. 6 shows how different values of λ in training phase affect the attack model performance. We show that for smaller values of λ , RNN works poorly as the data in previous time steps are important to train the model, accurately capturing the desired attack dynamics. On the other hand, FNN works worse for very large values of λ .

| SR % FNN/RNN | $\alpha = .5$ | $\alpha = 1$ | $\alpha = 2$ | $\alpha = 4$ | $\alpha = 8$ | $ \theta = \frac{\pi}{8}$ | $ \theta = \frac{\pi}{4}$ | $ \theta = \frac{\pi}{3}$ | $ \theta = \frac{\pi}{2}$ |
|-----------------|---------------|--------------|--------------|--------------|--------------|----------------------------|----------------------------|----------------------------|----------------------------|
| $\lambda = .01$ | 100/12 | 100/2 | 100/1 | 50/1 | 0/0 | 100/1 | 50/1 | 0/0 | 0/0 |
| $\lambda = .05$ | 100/98 | 100/97 | 100/90 | 58/0 | 0/0 | 100/92 | 53/0 | 0/0 | 0/0 |
| $\lambda = .1$ | 100/98 | 100/97 | 100/91 | 73/38 | 0/0 | 100/93 | 55/45 | 0/8 | 0/0 |
| $\lambda = 1$ | 100/100 | 100/100 | 100/70 | 97/59 | 0/0 | 100/75 | 100/60 | 54/3 | 0/0 |
| $\lambda = 5$ | 100/100 | 100/100 | 100/100 | 70/67 | 0/0 | 100/100 | 90/78 | 10/27 | 0/0 |
| $\lambda = 100$ | 100/100 | 100/64 | 100/42 | 0/12 | 0/0 | 100/43 | 1/16 | 0/0 | 0/0 |

Figure 6: Attack success rate (SR) for different values of λ with $T = 100$, $N = 200$ and different values of α and θ over 100 experiments for the inverted pendulum. The FNN/RNN numbers denote FNN vs RNN success rate values

Table 2: Attack success rate (SR) for different values of N with $T = 300$, $\lambda = .5$ and different values of y over 100 experiments for AV

| SR % FNN/RNN | $ y = .2$ | $ y = .6$ | $ y = .8$ | $ y = 1.2$ | $ y = 1.5$ | $ y = 2$ | $ y = 3$ | $ y = 4$ |
|-----------------|------------|------------|------------|-------------|-------------|-----------|-----------|-----------|
| $N = 1$ | 100/53 | 75/3 | 75/1 | 75/0 | 73/0 | 0/0 | 0/0 | 0/0 |
| $N = 10$ | 100/50 | 100/41 | 100/32 | 100/18 | 100/12 | 0/6 | 0/1 | 0/0 |
| $N = 50$ | 100/99 | 100/99 | 100/99 | 100/99 | 100/99 | 100/99 | 0/57 | 0/0 |
| $N = 100$ | 100/100 | 100/100 | 100/100 | 100/100 | 100/100 | 100/100 | 21/100 | 0/0 |
| $N = 500$ | 100/100 | 100/100 | 100/100 | 100/100 | 100/100 | 100/100 | 50/100 | 0/100 |

6.6 Autonomous Vehicle

We analyzed the impact of N , the MC sampling number during training, on attack performance in Table 2; we showed that for smaller values of N the FNN-based generator outperforms the RNN model. However, as N increases both models can perform equally good and even RNN performs slightly better.

6.6.1 Details of Employed CARLA Setup

For planning, CARLA provides with a state-machine waypoint following algorithm. A vehicle’s (estimated) pose and velocity are used along with map-based waypoints to coordinate (i) road-following, (ii) left-turn, (iii) right-turn, (iv) intersection, and (v) hazard-stop conditions [6]. We estimate the pose and velocity using an EKF with high-rate sensor data.

We also leverage the EKF structure to design an industry-standard chi-square anomaly detector. We set threshold η to have $\epsilon = .05$ in normal condition. Then, the integrity value shown in the left bar of Fig. 3a, 3b and 3c represents the number of measurements that pass the chi-square AD requirement out of the last 20 measurements. We assume that the attack is detected if more than two sensor measurements cannot pass the requirement in this window of time. As sensor inputs, a Global Navigation Satellite Sensor (GNSS) sensor provides loosely coupled position solutions in global coordinates, a commercial GNSS standard. We similarly define a generalized velocimeter model, derived from Doppler (or, more frequently in safety-critical applications, GNSS delta-range). State estimates and planning objectives are feed into a standard feedback controller [7] that targets a cruising speed of 25 km/hr ($\sim 7m/s$). The control algorithm drives the following actuators with associated input ranges: (i) Steering wheel angle on $[-1.0, 1.0]$, (ii) Throttle on $[0.0, 1.0]$, and (iii) Brake on $[0.0, 1.0]$. Finally, we visualize the vehicle trajectory and system integrity with a heads-up-display presented in Fig. 4 – the videos for our CARLA experiments are available at [1].

6.7 Unmanned Aerial Vehicles

Finally, we consider a quadrotor with complex highly nonlinear model from [2] which has twelve states $[x, y, z, \psi, \theta, \phi, \dot{x}, \dot{y}, \dot{z}, \dot{\psi}, \dot{\theta}, \dot{\phi}]^T$; x, y and z represent the quadrotor position along the X , Y and Z axis, respectively, while \dot{x}, \dot{y} and \dot{z} are their velocity. ψ, θ and ϕ are yaw, pitch and roll angles respectively, and $\dot{\psi}, \dot{\theta}$ and $\dot{\phi}$ represent their corresponding angular velocity. The system is sampled using Euler method with $T_s = .01s$. It is assumed that the states $[x, y, z, \psi, \theta, \phi, \dot{\psi}, \dot{\theta}, \dot{\phi}]^T$ are measured and are affected by zero-mean Gaussian noise with the covariance matrix $R = .01I$. We

Table 3: Attack success rate (SR) for different values of T with $N = 300$, $\lambda = .5$ and different values of α over 100 experiments for UAV

| SR % FNN/RNN | $\alpha = .2$ | $\alpha = .5$ | $\alpha = .7$ | $\alpha = 1$ | $\alpha = 3$ | $\alpha = 5$ | $\alpha = 7$ | $\alpha = 9$ |
|-----------------|---------------|---------------|---------------|--------------|--------------|--------------|--------------|--------------|
| $T = 100$ | 100/100 | 100/87 | 89/49 | 0/6 | 0/0 | 0/0 | 0/0 | 0/0 |
| $T = 200$ | 100/100 | 95/58 | 65/53 | 32/7 | 0/0 | 0/0 | 0/0 | 0/0 |
| $T = 400$ | 100/100 | 100/100 | 100/100 | 67/100 | 0/21 | 0/0 | 0/0 | 0/0 |
| $T = 600$ | 100/100 | 100/100 | 100/100 | 100/100 | 80/63 | 4/9 | 0/0 | 0/0 |
| $T = 800$ | 100/100 | 100/93 | 100/91 | 100/91 | 99/83 | 86/68 | 69/57 | 53/43 |

Table 4: Attack success rate (SR) for different values of T with $N = 300$, $\lambda = .5$ and different values of x along X axis over 100 experiments for UAV

| SR % FNN/RNN | $ x = .2$ | $ x = .4$ | $ x = .6$ | $ x = .8$ | $ x = 1$ | $ x = 1.5$ | $ x = 3$ | $ x = 4$ |
|-----------------|------------|------------|------------|------------|-----------|-------------|-----------|-----------|
| $T = 100$ | 93/50 | 1/2 | 0/0 | 0/0 | 0/0 | 0/0 | 0/0 | 0/0 |
| $T = 200$ | 47/5 | 17/0 | 5/0 | 1/0 | 0/0 | 0/0 | 0/0 | 0/0 |
| $T = 400$ | 100/57 | 44/14 | 0/5 | 0/0 | 0/0 | 0/0 | 0/0 | 0/0 |
| $T = 600$ | 83/78 | 66/24 | 50/4 | 37/2 | 30/1 | 13/0 | 0/0 | 0/0 |
| $T = 800$ | 97/77 | 90/36 | 85/22 | 75/13 | 68/10 | 51/1 | 0/0 | 0/0 |

Table 5: Attack success rate (SR) for different values of T with $N = 300$, $\lambda = .5$ and different values of y along Y axis over 100 experiments for UAV

| SR % FNN/RNN | $ y = .2$ | $ y = .5$ | $ y = .8$ | $ y = 1$ | $ y = 2$ | $ y = 4$ | $ y = 6$ | $ y = 8$ |
|-----------------|------------|------------|------------|-----------|-----------|-----------|-----------|-----------|
| $T = 100$ | 0/44 | 0/0 | 0/0 | 0/0 | 0/0 | 0/0 | 0/0 | 0/0 |
| $T = 200$ | 92/91 | 24/20 | 0/0 | 0/0 | 0/0 | 0/0 | 0/0 | 0/0 |
| $T = 400$ | 2/100 | 0/100 | 0/96 | 0/93 | 0/25 | 0/0 | 0/0 | 0/0 |
| $T = 600$ | 99/100 | 94/97 | 92/95 | 91/94 | 73/66 | 0/0 | 0/0 | 0/0 |
| $T = 800$ | 100/91 | 98/91 | 96/91 | 95/90 | 88/81 | 73/65 | 62/51 | 45/41 |

assume standard disturbance on the input modeled by system noise with zero mean Gaussian with the covariance matrix $Q = .001I$. We also set η such that $\epsilon = .01$.

we consider the position control task [2], where the drone should reach a predefined height (10m) and stay there (i.e., stay at coordinates $X = 0$, $Y = 0$ and $Z = 10$ if the initial point is denoted as $(0, 0, 0)$). UAV control for this task is based on a standard feedback-based controller.

G_θ used for synthesizing the stealthy attack is two layer recurrent neural network with ReLU activation function and 55 neurons per layer. H_θ is also a two layer fully connected network with ReLU activation function and 55 neuron for each layer. First, we train both models with $N = 300$ MC samples, $\delta = .2$, $\lambda = .5$ and different values of training period T . Table 3-6 show the success rate (in percentage) of both attack models for each training period T and different values of α , $|x|$, $|y|$ and $|z|$; i.e., the drone's distance from the desired position along each axis). As summarized, increasing the attack duration helps driving the system towards the unsafe region (i.e., increasing $|x|$, $|y|$ and $|z|$).

Fig. 7a illustrates the deviation of the drone over time for a successful attack sequence with $T = 800$ and $N = 300$. The attack starts at $t = 0$ and the figure shows the trajectory of the deviation before the attack gets detected. We can see that over time, the drone's deviation from the desired position will increase. Fig. 7b shows the norm of the attack vector of both FNN and RNN models for three different trained models with $T = 200, 400$ and 600 before the attack detection. We can see that unlike adversarial machine learning where the norm of the attack is limited to be bounded, the stealthiness condition in CPS requires the norm of attack vector to gradually increase over time.

Table 6: Attack success rate (SR) for different values of T with $N = 300$, $\lambda = .5$ and different values of z along Z axis over 100 experiments for UAV

| SR % FNN/RNN | $ z = .2$ | $ z = .4$ | $ z = .6$ | $ z = .8$ | $ y = 1$ | $ z = 2$ | $ z = 3$ | $ z = 4$ |
|-----------------|------------|------------|------------|------------|-----------|-----------|-----------|-----------|
| $T = 100$ | 0/9 | 0/0 | 0/0 | 0/0 | 0/0 | 0/0 | 0/0 | 0/0 |
| $T = 200$ | 67/0 | 24/0 | 4/0 | 0/0 | 0/0 | 0/0 | 0/0 | 0/0 |
| $T = 400$ | 44/42 | 0/17 | 0/10 | 0/7 | 0/4 | 0/2 | 0/0 | 0/0 |
| $T = 600$ | 86/81 | 59/74 | 45/60 | 26/48 | 11/36 | 3/28 | 0/3 | 0/0 |
| $T = 800$ | 95/88 | 88/85 | 78/83 | 69/80 | 64/75 | 40/66 | 0/41 | 0/6 |

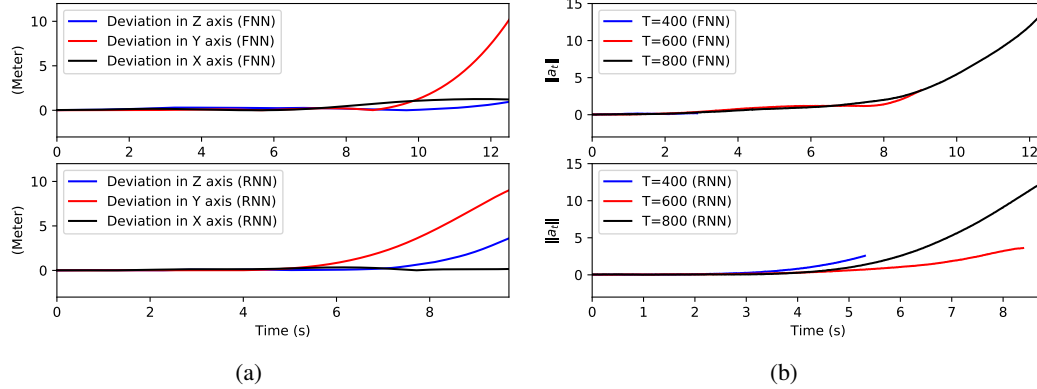


Figure 7: UAV altitude control: (a) The deviation of the drone along each axis from the desired coordinates $X = 0$, $Y = 0$ and $Z = 10$, for RNN and FNN-based attack (the attack starts at time zero); (b) The norm of the attack vector over time for both FNN and RNN methods with $T = 400, 600, 800$ before the detection of the attack.

6.8 Computational Resources

The workstation used for training is powered by Nvidia RTX 6000 graphics cards with 24 GB of memory each, two Intel Xeon Silver 4208 CPUs with 16 cores each and a total of 192 GB RAM. The code was developed using Python and Pytorch deep learning libraries.